



This project has received funding from the European Union's Horizon 2020 research and innovation programme under the Marie Skłodowska-Curie grant agreement No 645704

Modelling Mineral Foam Morphology Dynamics for Stability and Insulation Properties

Albrecht Gilka-Bötzow¹, Neven Ukrainczyk² and Eduardus A.B. Koenders³

ABSTRACT: Mineralized foam is an upcoming cementitious material that can be used as a sustainable building material. In view of recycling potential mineral foam has a cementitious microstructure that makes it a “clean” recyclable material. Designing mineral foam is a technology that demands control of the foam structure and the foam stability. From its basic state, mineral foam has an instable morphology that is continuously changing as long as the foam bubbles didn’t got frozen by setting/hardening of cementitious paste. This principle is making the material sensitive for its bubble and pore structure. In this paper, a schematic model is presented with which the bubble morphology and its associated foam stability can be simulated. The foam morphology dynamics was described by merging of different model foam structures having different characteristic bubble sizes, mixed in various volumetric ratios. A linear relationship was found between the degree of merging of different foam structures and the maximum bubble diameter in the foam system. The model turned out to have a great potential in making mineral foam predictable and designable.

1 INTRODUCTION

Mineralized cementitious foam is a still more upcoming material that can be used as a sustainable insulation material for in-situ or prefabricated plate applications. Mineral foams may replace commonly used hydrocarbon-based or glass-fiber based insulation products that are susceptible to fire and difficult to recycle. Cementitious foam is a poly-disperse system, consisting of gas bubbles, separated by cement paste layers, which stabilizes by "freezing" its (instable) structure at a certain moment in time, until set. A successful use of these cementitious foams asks for a continuous control of the instable foam morphologies, which is affected by various dynamic processes tending to equilibrate the forces between internal lamellar and bubble pore structure. The stable structure can be optimized mainly by an interaction between foam viscosity, which governs the rate of morphological changes, and the continuing binding of the cement paste until set. A research project has been conducted at the Institute of Construction and Building Materials of the TU Darmstadt, emphasizing the ability to control the processes which govern these foam instabilities. A morphology-based model has been developed with which the bubble structure and distribution of the lamellas can be schematized and which can be used to simulate the instabilities that develop inside a mineral foam. The so called octagon-quadrat model enables a predefined design of mineral foams and allows for an optimization of the thermal insulation capacity as well. Model backgrounds will be discussed and results will be presented and compared with experimental data.

¹ Dr.-Ing. Dott. Mag., Institute of Construction and Building Materials (WiB), Technische Universität Darmstadt, gilka-boetzow@wib.tu-darmstadt.de

² Dr. Chem. Ing., Institute of Construction and Building Materials (WiB), Technische Universität Darmstadt, ukrainczyk@wib.tu-darmstadt.de

³ Prof. Dr.ir., Institute of Construction and Building Materials (WiB), Technische Universität Darmstadt, koenders@wib.tu-darmstadt.de

1.1 Foam

Foam is a gas dispersion in a fluid or solid continuous phase [1]. The ISO 862 defines foam as a sequence of gas cells which are divided⁴ by thin fluid films. The confined gas volume is dispersed in a relatively small⁵ amount of liquid [4]. Like every system of non-miscible phases, foams aren't thermodynamically stable. The basic components tend toward separation and destabilization. Foam is, therefore, a multiphase system with a limited period of persistence [5]. The structure of fluid foams changes continuously because the surface potential tends to a minimum, by minimizing the interfaces between the phases while releasing the stored energy. Surfactants initialize the foam structure, but immediately after its formation begins the destruction [6]. There are several processes inside a foam which cause its destruction (fig. 1) [7].

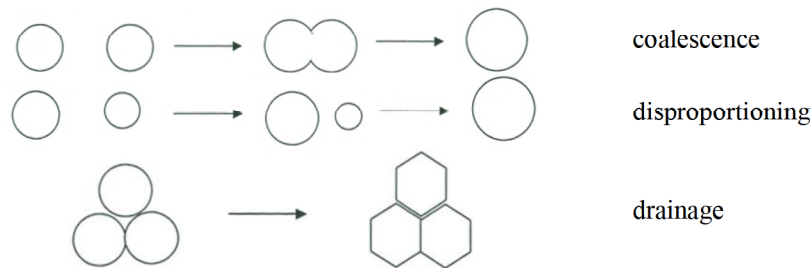


Figure 1: Process of foam destruction [8].

As shown in fig. 1, the structure of foam is significantly determined by the actual fraction of gas: ranging from gas emulsion ($< 54\%$ gas), over the spherical foam ($54\% < \text{gas} < 74\%$) up to polyhedral foam ($> 74\%$ gas). The specific weight can be a good criterion for characterizing a foam [9]. For aqueous foams, finding the right density is very often a point of scientific discussions [10]. Heavy foams tend to drain but are more flowable [11]. But when using them, more water is brought into the mineral foam with corresponding consequences for the cementitious matrix. Lighter aqueous foams are relatively stiff which becomes more explicit in case of applying an overdosage of foaming agent. This may lead to problems for getting foams with a constant void content [11]. Furthermore, the thin lamellas of a light foam with a low water content provoke a lower robustness of the aqueous foam against suction effects i.e. caused by cement particles [16]. Normal densities of the aqueous foams used for mineral foam production range between 60 kg/m^3 and 80 kg/m^3 [12].

The here discussed foamed cementitious materials are based on an aqueous foam principle, which is produced with a foam generator. This device merges the three essential substances, water, air and surfactant, into a fresh foam. The concentration of the foam agent can be changed by adjusting the flow ratio between the inflowing water and air phases. In an air intrusion device, using compressed air, the gas gets merged in the continuous phase and enclosed by the aqueous foam (cf. fig. 2) [13]. A porous membrane follows the air intrusion flow leading to a homogenized pore size distribution of the aqueous foam [5]. Here the pores in the accelerated foamed fluid get divided by the shear forces induced by the obstacles [14].

⁴ Open porous materials don't have a dispersed phase therefore they aren't foams within this definition [2].

⁵ Foams with a high gas volume are called colloid agglomerated gas dispersion, otherwise it is by definition no foam but an emulsions of gas [3].

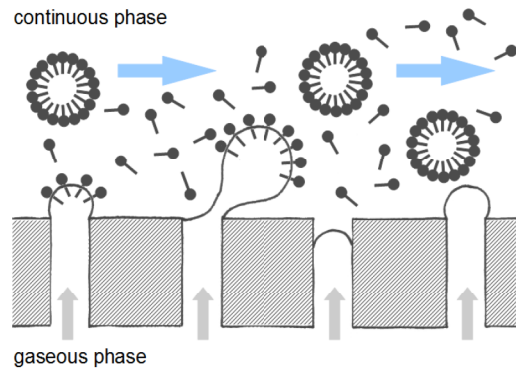


Figure 2: Model representation of a foam generation, forming bubbles into the foam via a perforated plate [13].

1.2 Foam concrete and mineralized foam

Foam concrete means a highly porous⁶ cementitious material without coarse aggregates⁷ [17, 18]. In contrast to autoclaved aerated concrete, foam concrete hardens due to cement hydration. Besides, the two material types show different characteristics in the hardened state [19]. It's possible to differentiate between the various types of foam concrete using dry density or composition. In addition, the used production technique is formative for their characteristics [20]. The publications analyzed in our Meta-study [21, 22] showed many parallels when referring to the different ranges of densities, and when referring to the fact that these ranges were in most cases between 100 kg/m³ and 500 kg/m³ (cf. fig. 5). On the one hand this can be related to the fact that researches were used to specific compositions or, on the other hand, that when producing foam concrete – even in the lab – it is very hard to meet exactly the specified design density [23]. This shows the need to classify different types of foam concrete [24].

Typically the highest density discussed is about 1800 kg/m³. This density is slightly lower than the 2000 kg/m³, which is the normative limit of lightweight concrete [16]. The foam concretes ranging between 1400 kg/m³ and 1800 kg/m³ are often reinforced and find their use in housing or soil applications, however almost always outside Europe [20, 25]. For these particular application, in Europe the more expensive lightweight aggregates concrete is normally used. The densities of the second category of foamed cementitious material range approximately between 800 kg/m³ and the priory mentioned 1400 kg/m³. It is used for structural applications but mostly as fillers or plugs in the mining or tunneling industry [26]. This material can, therefore, also be called ‘foam mortar’. A third category used as a robust filler or insulation material has a density of around 400 kg/m³ to 800 kg/m³. This class can be considered to be part of the mineral (fresh state) or mineralized (hardened state) foams [27]. All other types of foams, with densities below a dry density of 400 kg/m³ are called lightweight mineral foams and/or mineralized foams, respectively. This type of foam is a relatively new subject that still requires a research effort, and is mostly used as an insulation material (tab. 1) [28].

⁶ The porosity normally is way higher than in an air-entrained concrete [15].

⁷ For this reason actually it is not really correct to define it a concrete. It would be better to speak from foam mortar or rather mineralized foam [16].

Table 1. Dry density ranges and proposed categorization for porous cementitious foams with aggregates $D < 2$ mm.

dry density range [kg/m ³]	category
1400 – 1800	(reinforced) foam concrete
800 – 1400	foam mortar
400 – 800	mineralized foam
< 400	lightweight mineralized foam

All foamed cementitious materials discussed in this context are essentially a mix of aqueous foam and a binder matrix. This technique has the methodical advantages that all components can be individually admeasured and analyzed before mixing. This makes the calculation of the mass flow more transparent, and interdependencies between the used materials can be easily identified and considered. Thus for production a three step procedure was used. First the binder paste is produced in a specific mixer such as a mortar or slurry mixer, which ensures a homogenous paste due to the high shear forces [47, 48]. Next, the foam is generated as mentioned before. Finally, both components are mixed together in a classical concrete mixer.

2 TEST PROCEDURES

2.1 Visual classification of mineralized foam structure

Comparative visual studies on the foam structure of solidified mineralized foams allowed for a unique identification and classification. Such indicative evaluation could initially only be done to those foam classes which are visible with the naked eye. In this case distinction can be made between the average maximum bubble diameters, homogeneity of the bubble size distribution as well as the robustness of the bubble lamellae (double layered membrane) that form the morphological framework of a mineral foam. Poor, or too thin lamellae can result in a bad bubble size distribution or in a substantial lack of meso-bubbles being formed in the foam. From the initial tests, it was possible to identify 4 typical foam structures, which are exemplary provided in figures 3 to 6.

It is important to know that the proposed classification of foam classes not unconditionally coincide with the variation of the water cement ratio. Considered differences may, therefore, be attributed to slight differences in age of the used cements, to the two different mixing techniques or to differences in the level of energy needed to mix the cement pastes. This supports the desire for a more direct relationship between the foam properties and the properties of the cement paste rheology.

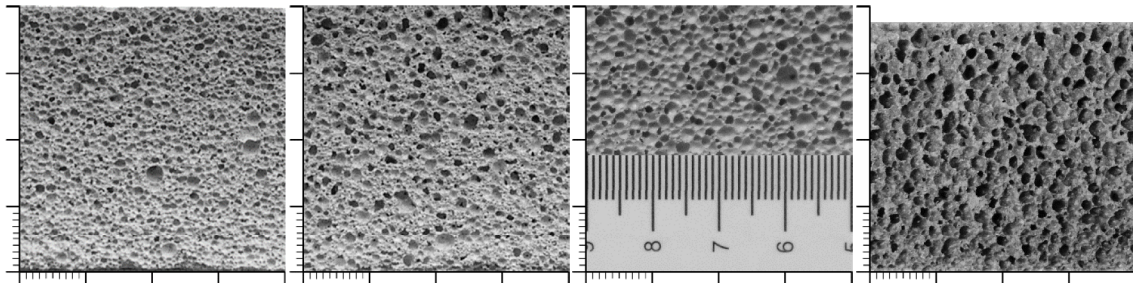


Figure 3: Foam class B, Scale 1 mm (Sample ID B1045).

Figure 4: Foam class A, Scale 1 mm (Sample ID B4A035).

Figure 5: Foam class C, Scale 1 mm (Sample ID AVe3040).

Figure 6: Foam class D, Scale 1 mm (Sample ID AD2050).

For the foam classes shown in figures 3 to 6, the following observations can be made: foam class A has similar characteristics as foam class B, but with a larger maximum bubble diameter of about 1.5 mm (fig. 4). Foam class B shows a homogenous pattern of uniformly distributed macro-pores with a maximum diameter of about 1 mm (fig. 3). Foam class C shows a clear distribution of pores with very fine lamellae, leading to a smaller range of bubbles available in the system, i.e. mostly equally sized bubbles having a maximum diameter of about 2 mm (fig. 5). Foam class D shows similar bubble characteristics as foam class C, however, with tendency of the bubble to merge in a later stage of the hydration process. This results in irregular and clearly larger pores relative to the largest bubble diameter. In addition, an enhanced tendency of bubble collapse could be observed (fig. 6).

When considering all foam classes, it can be seen that there is a clear tendency towards the formation of a polyhedral structure, depending on the bubble size and foam class. It shows a lower share of smaller bubbles for an approximately similar total pore volume, resulting in a lower volume of continuous lamellae (fig. 7). The structure will alter from a densely packed formation of spherical bubbles to a polyhedral bubble structure in which most of the cement paste volume is located in the lamellae instead of being located in the nodes (forming bulk volume of the continuous phase).

In addition, it can be considered that the relationship between the achieved dry density and wet density, regardless of the pore structure type, varies between 0.61 and 0.73. Deviations from the targeted wet density mostly run to lower values. A deviation from the wet density up didn't occur in the foam structures of class C. An exception are the foam structures classified in group D, which showed a different behavior in the production of the tested foams. In this case, the cement paste was added in two steps, in order to exactly achieve the wet density as was aimed for.

2.2 Classification of the pore size distribution

There are three main types of pores: C-S-H gel pores (< 30 nm), capillary pores (30 nm – 10 μ m) and foam bubbles (> 10 μ m). Because of the characteristic wide range of differently sized pores, microscopy and mercury intrusion porosimetry (MIP) techniques were combined to characterize the overall pore size distribution. The MIP measurements were carried out with Pascal 440 from Thermo-Scientific. The volume of mercury, which penetrates the sample, is a function of the applied hydrostatic pressure (up to 400 MPa). The pore diameter is determined with the Washburn equation. Mercury properties are: density 13.53 g/cm³, surface tension 0.485 N/m, and contact angle 130 °. The measurements were performed with gradual reading for each applied pressure (increase speed of about 10 MPa/min), on the previously dried sample with an evacuation pressure of 50 μ m Hg during 5 minutes.

With the classification method used to evaluate the bubble size distribution of the particular foam classes it is possible to identify the pore sizes for different paste, mixing and casting conditions. With this, for the first four classes A to D (fig. 3 to 6) addressed before, this results in the evaluated pore size distribution as provided in figure 7.

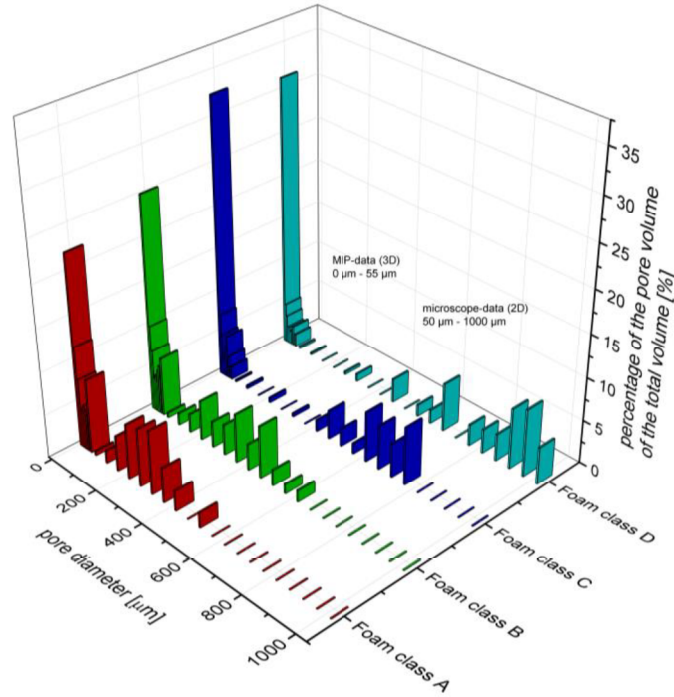
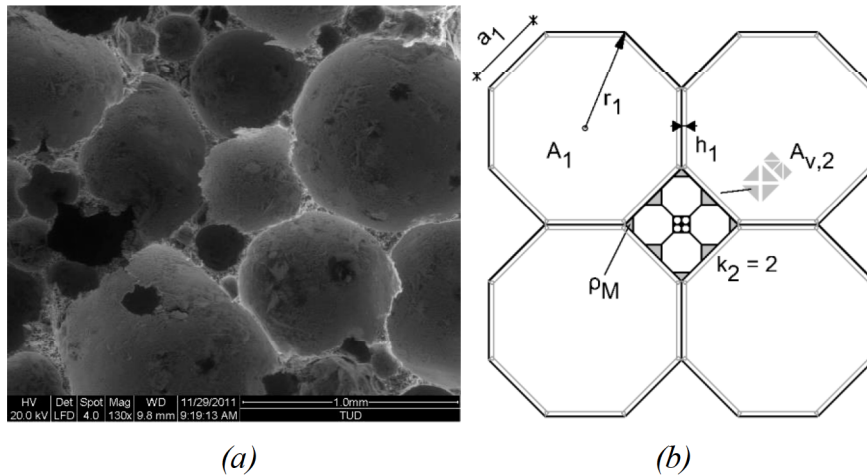


Figure 7: Pore size distribution for the foam classes A to D (fig. 3 to 6) ranging from 0 to 1000 μm .

3 OCTAGON-QUADRAT-MODEL

Cementitious foam is a material that is in a continuously changing state that never reaches total equilibrium situation until hydration has evolved so far that it “freezes” a certain state of bubble development, which is neither monodisperse nor perfectly polyhedral (fig. 8a). To schematize this complex morphology of bubble clusters, a two dimensional modelling approach consisting of an octagons and quadrat configuration has been developed (fig. 8b). The proposed model allows for a realistic distribution of the masses over the geometrical bubble structure, where a certain portion of the mass is assigned to the bubble surfaces and a remaining portion to the nodes in between the bubbles, leading to a configuration which is capable of simulating building physics properties as well.



(a) SEM-Picture of a mineralized foam
(b) two-dimensional octagon-quadrat-model

Table 2. Relevant geometrical dependences in an octagon [29].

Variable	Formula	Number
edge length	a_n	(a)
perimeter radius	$r_n = \frac{a_n}{\sqrt{2-\sqrt{2}}}$	(b)
perimeter diameter	$D_n = 2 \cdot r_n$	(c)
inscribed area	$A_n = a_n^2 \cdot (2 + 2 \cdot \sqrt{2})$	(d)
total edge length	$U_n = 8 \cdot a_n$	(e)

A minimum of one octagon and one quadrat are necessary to develop the model mathematically (fig. 8b). Inside the first quadrat and along the edge of the first octagon ($n = 1$) there are more octagons ($n = i + 1$) with a dividing factor k_{i+1} and an edge length a_{i+1} ; their quantity is $(k_{i+1})^2$. The index n is the level and the resolution of the mathematic model. Thus there can be next to every octagon a quadrat which is filled with smaller octagons. However following the perception of a node between foam bubbles the last quadrat is totally filled with cement paste material. Apart from this, there is also distributed mass inside the corners between the octagons and along their edge.

In this way the bubble size distribution can be a function of k_i . The length of the longest edge a_l can be derived from the biggest pore radius or diameter (eq. b and c). All other levels of the model depend on in each case higher level (eq. f). All indices are positive and in whole numbers.

$$(D, a)_{i+1} = \frac{(D, a)_i}{k_{i+1} \cdot (1 + \sqrt{2})} \quad (f)$$

D_i : octagon diameter.

a_i : octagon edge length.

k_i : dividing factor of the octagon i ; where $k_1 = 1$

The mass of the continuous phase is distributed over the total length of the octagon surfaces with thickness h_i , meaning that those surfaces where the octagons touch the total thickness of the surface will be $2h_i$, being the summation of the mass from 2 octagons. The overlaps of the schematized surface thickness at the corners is neglected (fig. 8 b). In order to reduce the number of input parameters, the surface thickness h_i was related to the octagon radius r_i with a ratio t (eq g).

$$h_i = \frac{r_i}{t}, \text{ where } t \geq 1 \quad (g)$$

Hence, the surface area of the octagons will be (eq. h):

$$A_{b,i} = U_i \cdot h_i = \frac{8a_i^2}{t\sqrt{2-\sqrt{2}}} \quad (h)$$

The area of the nodes with the lumped mass is (eq. i):

$$A_{v,i+1} = a_{i+1}^2 \quad (i)$$

h_i : octagon edge thickness.

r_i : octagon (bubble) radius.

a_i : octagon edge length.

$A_{b,i}$: octagon surface area.

$A_{v,i}$: mass filled node between two octagons.

t : ratio of octagon radius and edge thickness.

These formulas enable the calculation of the total mass distribution over the octagons and with this the calculation of the specific density of the schematized foam (eq. j).

$$\rho = \rho_M \cdot \frac{\sum_{i=1}^n [k_i^2 \cdot A_{b,i}] + \sum_{i=2}^{n-1} [(2 \cdot k_i - 1) \cdot A_{v,i}] + k_n^2 \cdot A_{v,n}}{A_O + a_1^2} \quad (j)$$

The three-dimensional character of the schematized foam model is achieved by simply adding a height to it. This is done while an octagon cannot be transferred into a regular polyhedral [1]. Based on the geometrical coherence of the system this height has to be equal to the diameter of the pore which is represented by the octagon (eq. c). With this approach, the number of elementary cells ($i+1$) in the third dimension g_{i+1} are not in a whole number (integer) relationship with the pore diameter of the octagon i (eq. k and l).

$$g_{i+1} = \prod_{i=1}^n \frac{r_i}{a_i} \quad (k)$$

From this, and analogue to equation j can the three dimensional Octagon-Quadrat-Model be described as (eq. l).

$$\rho = \rho_M \cdot \frac{A_{b,1} \cdot r_1 + A_{O,1} + \sum_{i=2}^n [(k_i^2 \cdot A_{b,i} \cdot r_i + A_{O,i}) \cdot g_i]}{A_O + a_1^2} + \rho_M \cdot \frac{\sum_{i=2}^{n-1} [(2 \cdot k_i - 1) \cdot A_{v,i} \cdot a_i \cdot g_i] + k_n^2 \cdot A_{v,n} \cdot a_n \cdot g_n}{A_O + a_1^2} \quad (l)$$

- ρ_M : dry density of the binder matrix.
 $A_{b,i}$: edge area of the octagon.
 $A_{O,i}$: surface of an octagon.
 $A_{v,i}$: mass filled node and corners between the smallest octagons.
 a_i : octagon edge length
 r_i : perimeter radius.
 g_{i+1} : number of elementary cells starting from level $n = 2$.
 k_i : dividing factor of the octagon or number of octagons i .

Hence, for any maximum bubble diameter and with incorporation of a prescribed type of micro-porosity indicate by k and/or n , the density of the mineral foam matrix ρ_M can be adapted (fig. 9).

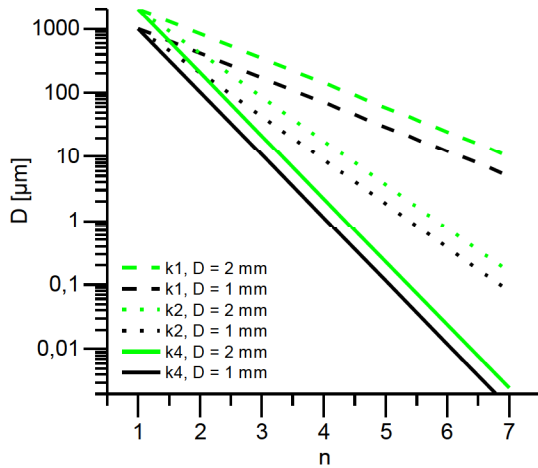


Figure 9: Pore diameter in the Octagon-Quadrat-Model for model level n , and for constant $k = 1, 2$ and 4 $D_1 = 1$ mm und 2 mm.

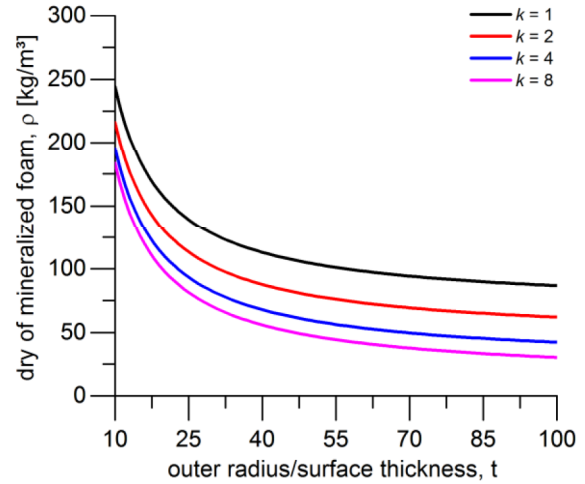


Figure 10: Octagon-Quadrat-Model, density of mineral foam (eq. j) relative to the distribution factor between the outer radius and the surface thickness (eq. g), for different division factors k , solved for a pore size reduction of $n = 7$, $\rho_M = 1950 \text{ kg/m}^3$.

Based on the formulas derived for the initially two-dimensional octagon-quadrat model, in fig. 10 the specific density of a poly disperse mineral foam is determined for a predefined division factor for the outer radius h_i and surface thickness t_i . In this example, the calculations were done for a octagon division factor $n = 7$, meaning that the pore cluster in the node of the four octagons were repeated 7 times to reach agreement with the smallest pore size in the mineral foam system.

The shape of the calculated curve is independent from the initial octagon diameter D_1 , which indirectly affects the entire bubble size distribution as described by eq. j. Because of this, the surface thickness reduces proportionally to the size of the representative pore. For higher division factors k , the small pores dominate. Proportional to this, the model shows lower densities for these ranges of pore sizes (fig. 10)

Figure 11 shows the simulated and via measurements determined cumulative volume fractions in connection with their relative bubble size distribution. Moreover, it shows similar relationship calculated with the two dimensional Octagon-Quadrat Model for various division factors k (number of octagons). Even from the analyzed SEM images (fig. 8) it can be assumed that, for different pore diameters, the ratio of outer radius and surface thickness of the octagon t is nearly constant, regardless of the density and the type of foam. Accordingly, and based on the curves in figure 10, the selected division factor t has been chosen $t = 40$ (fig. 11).

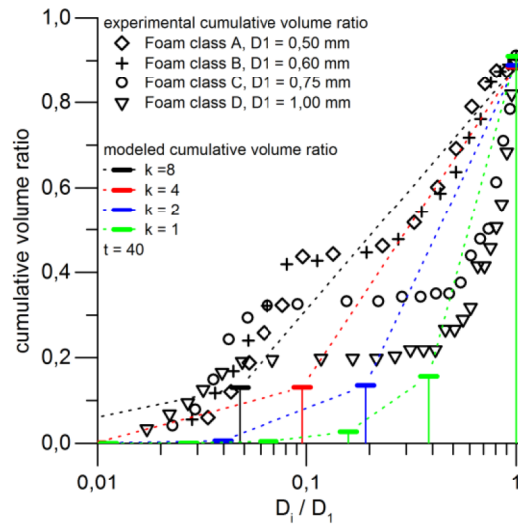


Figure 11: Measured and with the Octagon-Quadrat-Model simulated, cumulative Volume ratios in relation to the respective relative bubble size distributions. Modelled is the two dimensional approach for different division factors k , and radius/surface thickness factor $t = 40$.

In the analysis of the bubble distribution of the examined foams as provided in fig. 11 and 12, pore sizes smaller than $10 \mu\text{m}$ are not considered. The considered bubble volume accounts for approximately 60% to 65% of the total pore space. The model, already in this basic form, shows a reasonable agreement for the foams of classes C and D. However the foams with a finer bubble structure, i.e. class A and B, could not be modeled satisfactorily (fig. 3 to 6).

The experimental data in figure 7 shows a significant discontinuous gap between the relatively larger foam bubbles and micro-bubbles that are embedded in the cement paste

volumes. Both bubble ranges appear obviously as a merged system in a mixed (combined) foam bubble structure. This fact opens a way for an improved modeling where the Octagon-Quadrat Model also may include this merging of bubble classes. Based on previous observations, in fig. 12, two types of mineral foams, both with different bubble sizes are presented, while mixed in various volumetric ratios. In this figure, analogue to fig. 11, the measured data for the various foams are presented as well. The micro-bubbles include both capillary pores embedded in the cement paste and the smallest bubbles generated by the foam. This pore size range is largely stable and has been accepted in the model as constant, whereas the maximum bubble diameter has been set to 0.05 mm – 1.00 mm. The choice of the respective largest bubble size and the volume ration used for merging the two types of foams was depending on the bubble classes and was determined iteratively. For the foam bubbles of the respective foam classes a diameter D_1 of 0.5 mm, 1 mm and 1.3 mm was assumed. In addition, since the classes A and B showed quite a similar maximum bubble diameter, only one bubble size distribution was modelled. The dashed lines in the figure are drawn to show the relationship between the modeled points and to make the relations clearer and more explicit (fig. 12).

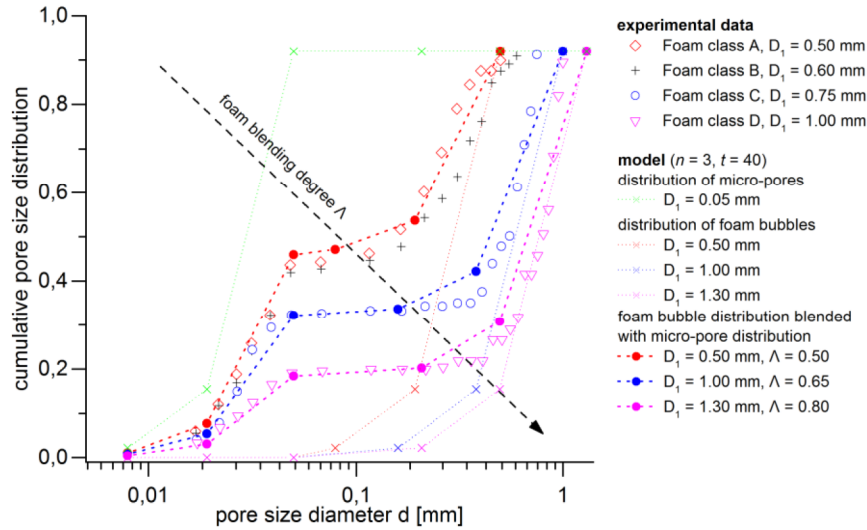


Figure 12: Measured data and results from the Octagon-Quadrat-Model, showing the cumulative volume ratios in relation to the bubble diameters, using a 2D model with $n = 3$, division factor $k = 1$ and $t = 40$, both consisting of a blend of two foam bubble size distributions with different volumetric fractions.

In contrast to the single micro-bubble size distribution the overall bubble size distribution is more time dependent, and shows more variation with the rheology and the evolution of the hydration process of the cement paste. This typically results in the different foam type classes. Fig. 12 indicates that the degree of merging Λ is proportional to the bubble classes of the foam, and thus with the degree of disintegration of the mineral foam. Whenever plotting the determined degree of merging Λ against the measured maximum pore diameter D_1 of the bubble classes, a linear relationship appears (fig. 13). With this, mineral foam can be classified based on its desired disintegration, and can, with the help of the Octagon-Quadrat-Model, determine the corresponding degree of merging. Along this line, with application of the Octagon-Quadrat-Model, the development of the instationary behavior of mineral foam structures can be evaluated.

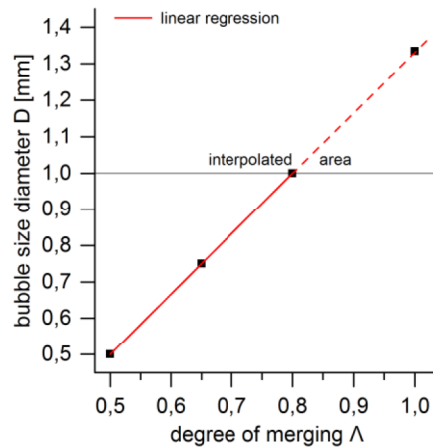


Figure 13: Experimentally determined bubble size diameter versus the degree of merging Λ with the Octagon-Quadrat-Model.

4 CONCLUSIONS

The proposed Octagon-Quadrat-Model provides an easy way to evaluate poly-disperse foam structures. In particular, the typical character of mineral foam where bubble classes are clearly distributed in two categories, viz. in relatively larger foam bubbles and in micro-bubbles, which can be included in the model explicitly. The model parameters (k , n , and l) represent the degrees of freedom that allows for modeling other typical foam structures. The smallest bubble sizes with their distribution and shape didn't had a significant effect on the results calculated with the Octagon-Quadrat-Model (see. fig. 7). The model can, in combination with rheological and calorimetrical (hydration kinetics) findings be the basis for a targeted design of a mineral foam. The proposed relationship between the degree of merging Λ and the maximum bubble size distribution can provide the possibility to show the thermodynamic related changes of a foam structure by applying the superposition of two Octagon-Quadrat-Models with different size characteristics. The achieved bubble size distributions can serve as the starting point for mechanical or building physics oriented simulations.

ACKNOWLEDGEMENT

The authors acknowledge support by H2020-MSCA-RISE-2014 project No. 645704 - SUSTAINABILITY-driven international/intersectoral Partnership for Education and Research on modelling next generation CONCRETE.

REFERENCES

- [1] Myers, D.: Surfactant Science and Technology. In: Berichte der Bunsengesellschaft für physikalische Chemie 96 (1992) pp. 1898–1898
- [2] Bikerman, J.: Foams. Springer-Verlag, New York (1973)
- [3] H. Mathes: Monodisperse Schäume: Herstellung und Verwendung als strukturiertes Medium für chemische Zweiphasenreaktionen. Universität Bremen (2004)
- [4] Deutsches Institut für Normung: DIN EN ISO 862:1995-10, Grenzflächenaktive Verbindungen - Begriffe, Beuth Verlag
- [5] Schilbach, J.: Entwicklung und Optimierung eines biotechnologischen Verfahrens zur Herstellung von Proteinschaummitteln. Technische Universität Hamburg-Hamburg (2005)
- [6] Tscheuschner, H.-D.: Grundzüge der Lebensmitteltechnik. Behr, Hamburg (1999)

- [7] German, J.: Properties of Stabilizing Components in Foams. In: Chem. Eng. (1990) pp. 62–70
- [8] Caessens, P.W.J.R.: Enzymatic hydrolysis of β -casein and β -lactoglobulin. Foam and emulsion properties of peptides in relation to their molecular structure. Wageningen University (1999)
- [9] Lohaus, L.: Konstruktionsleichtbeton unter Verwendung vorgeschäumter Luftporen. , Hannover (2005)
- [10] Pott, J.U.: Entwicklungsstrategien für zementgebundene Schäume. Universität Hannover (2006)
- [11] Lohaus, L.: Anwendbarkeit vorgeschäumter Luftporen im Betonbau. Fraunhofer-IRB-Verl., Stuttgart (2000)
- [12] Karl, S.: Leichtzuschlag-Schaumbeton als Konstruktionsleichtbeton mit abgeminderter Rohdichte. TU Darmstadt (1979)
- [13] Bals, A.: Verfahrenstechnik und Substratfaktoren beim Aufschäumen mit Membranen. VDI-Verl., Düsseldorf (2002)
- [14] Wilson, A.J.: Foams physics, chemistry and structure. Springer, London (1989)
- [15] Deutsche Bauchemie e.V. hrsg: Herstellung von Luftporenbeton, (2001)
- [16] Deutsches Institut für Normung: DIN EN 206:2014-07, Festlegung, Eigenschaften, Herstellung und Konformität, Beuth Verlag
- [17] Deutsches Institut für Normung: DIN 4164:1951-10, Gas- und Schaumbeton - Herstellung, Verwendung und Prüfung, Richtlinien - zurückgezogen, Beuth Verlag
- [18] Deutsches Institut für Bautechnik: DIBt Mitteilungen Nr. 6:2002-12, Herstellung und Verwendung von Schaumbeton, DIBt
- [19] Stegemann, R.: Das grosse Baustoff-Lexikon. Handwörterbuch der gesamten Baustoffkunde. Deutsche Verlags-Anstalt, Stuttgart (1941)
- [20] Ramamurthy, K., Kunhanandan Nambiar, E.K., Indu Siva Ranjani, G.: A classification of studies on properties of foam concrete. In: Cement and Concrete Composites 31 (2009) pp. 388–396
- [21] Albrecht Gilka-Bötzow: Betrachtung instationärer zementöser Schaumstrukturen. TU Darmstadt, Darmstadt (2016)
- [22] Gilka-Bötzow, A., Zimmer, M., Koenders, E.A.B.: Material Properties of mineralized foam and its density dependency - a meta-study. In: Proceedings of the int. Conf. on Concrete Sustainability (ICCS16) (2016)
- [23] Stark, J.: Dauerhaftigkeit haufwerksporiger Leichtbetone mit Schaummörtelbindung. Fraunhofer IRB-Verlag, Stuttgart (2003)
- [24] Global Construction: Ultimate Concrete Opportunitics (2005 : University of Dundee) creator: Use of foamed concrete in construction proceedings of the international conference held at the University of Dundee, Scotland, UK on 5 July 2005. Thomas Telford, London, UK (2005)
- [25] Kearsley, E., Booyens, P.: Reinforced Foamed Concrete-Can It Be Durable? In: Concrete Beton (1998)
- [26] Cox, L., van Deijk, S.: Foam concrete. In: Concrete 25 (2002) pp. 54–55
- [27] Akthar, F.K., Evans, J.R.G.: High porosity (90%) cementitious foams. In: Cement and Concrete Research 40 (2010) pp. 352–358
- [28] Gilka-Bötzow, A., Röser, F., Koenders, E.A.B.: Mineral Foam in Energy Active Buildings. In: RCCS Conference 2015 - Proceedings, Nagasaki, Japan (2015)
- [29] Barth, F., Krumbacher, G., Matschiner, E., Osslander, K. hrsg: Anschauliche Geometrie. Ehrenwirth, München (1988)